ACS APPLIED POLYMER MATERIALS

pubs.acs.org/acsapm Article

Healable and Transparent Ionic Conductive Hydrogels Based on PNATF as Multiple-Signal Sensors

Yan Liu,[1] Yirong Wang,[1] Yan Fu, Nan Nan Wang, Si Qi Zhan, Li Sheng, Hong Yu Yang,* and Changling Liu*

Cite This: *ACS Appl. Polym. Mater.* 2025, 7, 2529−2540 Read Online

ACCESS | Metrics & More | Article Recommendations | Supporting Information

ABSTRACT: In recent years, flexible wearable technology has been extensively utilized in health monitoring due to its capabilities of acquiring multiple signals and transmitting data wirelessly in real time. Ionic conductive hydrogels have already played an important role in the field of flexible wearable devices depending on their excellent biocompatibility, mechanical adaptability, and transparency. In this study, a multiresponsive ionic conductive hydrogel with both superior mechanical properties and self-healing ability was constructed through the interwoven network structure. The basic skeleton is formed by *N*-isopropylacrylamide and acrylic acid (PNIPAM/PAA) through co-cross-linking. The final interwoven structure is constructed by the network of ethylenediaminetetraacetic acid ferric (III) sodium salt cross-linked with tannic acid (TA) interpenetrating with the basic backbone. The stretchability of up to 2638% can be achieved due to the dynamic hydrogen bonding between the PNIPAM/PAA skeleton and TA. Meanwhile, the abundant catechol groups of TA endow the hydrogel with an adhesion strength of 7.06 kPa, and it can be easily peeled off without any residue when applied to the human skin. The stable mechanical cycling performance, outstanding self-healing ability, electrical conductivity (1.28 $S \cdot m^{-1}$), and sensitivity (GF = 4.368) of the hydrogel are attributed to the reversible coordination of Fe^{3+}. Based on the above comprehensive performance, the ionic conductive hydrogel designed in this study will have great application potential as a temperature-sensitive sensor in monitoring human movement and environmental temperatures, which also provides a unique perspective for the detection of fever and abnormal thermotherapy.

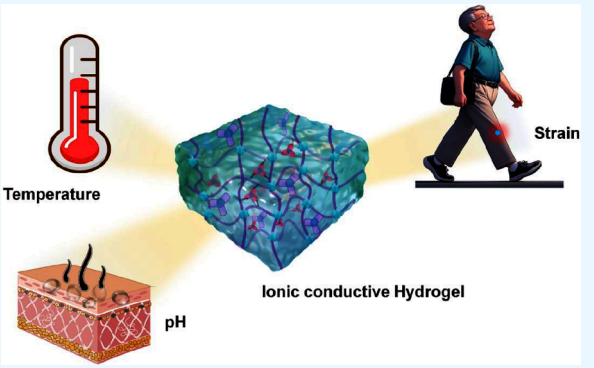

KEYWORDS: *ionic conductive hydrogel, interwoven network, self-healing, biosensor, multiple-response sensor*

INTRODUCTION

The wearable electronic devices have attracted more and more attention in the field of medical diagnosis, healthcare, soft robotics, e-skin, and motion detection.[1−5] However, the mismatched mechanical properties and biocompatibility of traditional electronic devices lead to weak signal transmission and limited physiological applications.[6,7] Conductive hydrogels that combine exceptional mechanical properties, high electrical conductivity, and biocompatibility have shown great advantages in flexible electronic sensors, as they can accurately convert mechanical deformations into electrical signals for monitoring human health.[8−11] Several methods have been developed to construct conductive hydrogels as wearable sensors, such as embedding either electronic conductive fillers (including metallic nanoparticles,[12−15] carbon-based materials,[16] and intrinsically conductive polymers[17,18]) and ionic conductive materials (such as solvated deliquescent salt[19−22] and ionic liquid[23−25]) within a three-dimensional hydrogel structure. Compared with rigid electronic fillers, ionically conductive hydrogels are more suitable as motion, UV, and temperature for monitoring human health attributed to their flexibility and transparency.[26−31] In addition, excellent temperature response and stability were exhibited in the ionic conductive hydrogels, which were attributed to their outstanding ionic transport properties.[32−36] For example, the conductive hydrogels with ionic cross-linking properties were successfully prepared by introducing a variety of ions and solvents into the polyacrylamide (PAM)/carrageenan dual network, which exhibit significant sensitivity in terms of temperature and strain.[37] However, the transport mechanism of ion-conducting hydrogels will be affected by various stimuli (strain, pH, and temperature), all of which can interfere with the sensing signal and reduce accuracy of health assessment.

Received: November 26, 2024
Revised: February 4, 2025
Accepted: February 11, 2025
Published: February 18, 2025

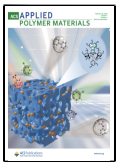

https://doi.org/10.1021/acsapm.4c03794
ACS Appl. Polym. Mater. 2025, 7, 2529−2540

Scheme 1. Design and Application of Multi-Signal Responsive PNATF Ion-Conducting Hydrogels as Flexible Wearable Sensors

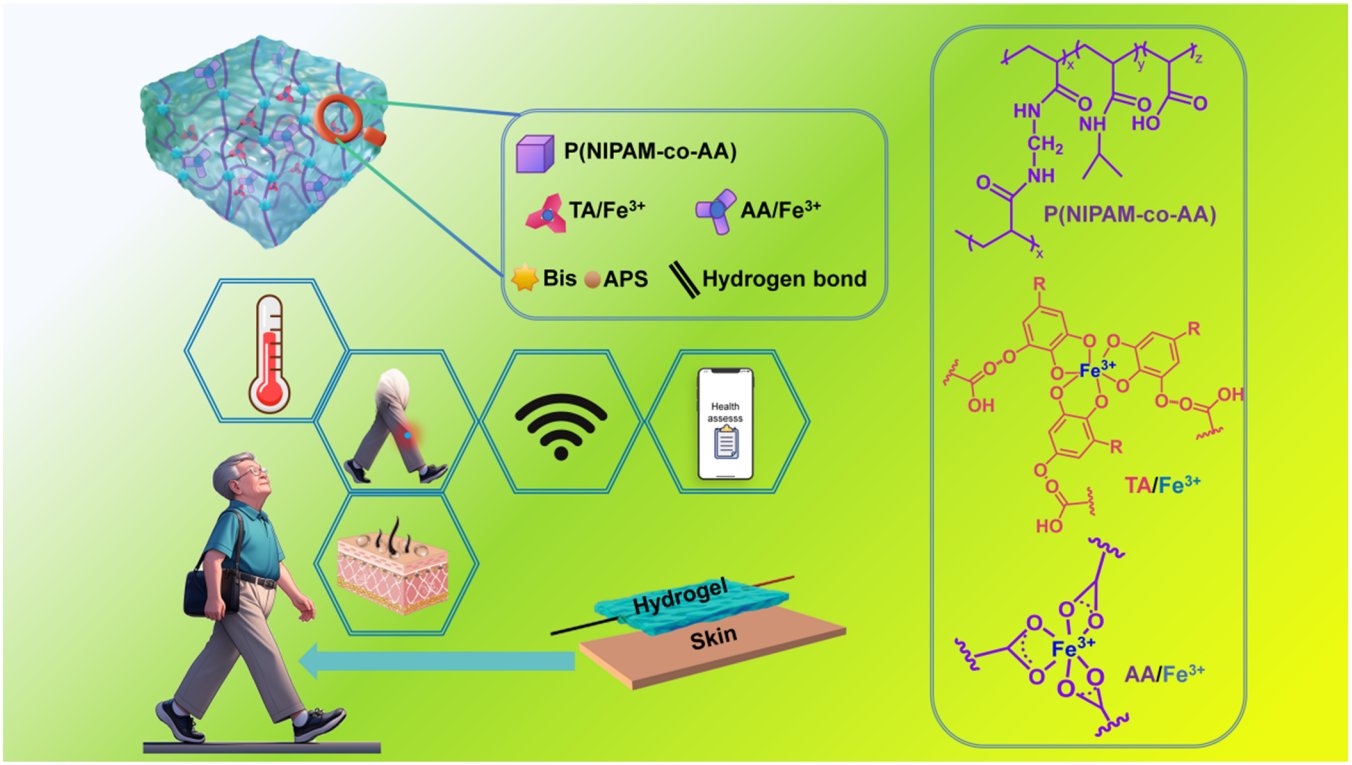

To address this issue, a multiple-signal sensor capable of independently responding to changes in temperature, pH, and strain was designed by integrating sensitive materials into ionic conductive hydrogels, which aims to identify the frailty of the elderly and monitor their disease changes in time.

Poly(*N*-isopropylacrylamide) (PNIPAM) is considered as a typical temperature-sensitive polymer due to its reversible discontinuous volume phase transition at approximately 32 °C,[38] showing great potential in the field of sensors.[39] For example, Han et al. prepared a self-healing hydrogel of PNIPAM with good tensile and conductive properties.[40] As a weak acidic polyanionic hydrogel with high ionic conductivity,[41−43] polyacrylic acid (PAA) will respond to pH stimuli.[44] At present, the research of PAA ion-conductive hydrogels as pH sensors has also attracted the interest of many scientists.[45,46] The carboxyl groups (−COOH) of the PAA hydrogel are present in their deprotonated form COO− under alkaline conditions, leading to hydrogel swelling. In contrast, the COO− groups are protonated upon exposure to acids, resulting in hydrogel shrinkage. The −COOH of the PAA hydrogel is present in deprotonated form (COO−) under neutral or alkaline conditions, leading to gel expansion. In contrast, the COO− group will become protonated when exposed to acids, resulting in hydrogel shrinkage.[47] However, the previously reported PNIPAM and PAA hydrogels have a difficult balance between high GF values and scalability, which poses a challenge for the fabrication of high-performance scalable electronics.[48,49] Phenyltriphenol and catechol groups on tannic acid molecules can form physical cross-links with polymers, such as hydrogen bonds, $\pi-\pi$ interactions, and hydrophobic interactions. When hydrogels are subjected to stress, these hydrogen bonds can be dynamically broken and recombined, effectively dissipating energy on the molecular scale. This improves the mechanical properties and enhances the ductility of the hydrogels.[50,51] Meanwhile, it can also complex with various metal ions, which not only enhances the conductivity and scalability of the material but also endows the hydrogel with multifunctionality.[52] It embodies extraordinary significance to investigate the structural design of above functional groups for the development of high-performance multiresponsive ionic conductive hydrogel. Although there have been a lot of studies on temperature and pH sensors, there are relatively few reports on sensors that can simultaneously detect multiple signals such as temperature, pH, and motion using ion-conductive hydrogels.

In this research, a multiresponsive transparent ionic conductive hydrogel (named as the PNATF hydrogel) with both superior mechanical properties and self-healing ability was constructed through the interwoven network structure. As shown in Scheme 1, the basic skeleton is formed by *N*-isopropylacrylamide and acrylic acid (PNIPAM/PAA) through co-cross-linking. The final interwoven structure is constructed by the network of ethylenediaminetetraacetic acid ferric (III) (EDTA) sodium salt cross-linked with tannic acid (TA) interpenetrating with the basic backbone. The outstanding mechanical properties and self-healing ability of the PNATF hydrogels were endowed by the cross-linking of Fe^{3+} with TA. The conductivity was improved by incorporating the two conductive ions (Fe^{3+} and Na^{+}) into the hydrogel simultaneously via ferrosodium EDTA. The rapid and stable response of hydrogels to pH, temperature, and strain was also verified. Therefore, the PNATF ionic conductive hydrogel will have great application potential as a temperature-sensitive sensor in monitoring human movement and environmental temperatures, which also provides a unique perspective for the detection of fever and abnormal thermotherapy.

https://doi.org/10.1021/acsapm.4c03794
ACS Appl. Polym. Mater. 2025, 7, 2529−2540

2. EXPERIMENTAL SECTION

2.1. Materials. *N*-Isopropylacrylamide (NIPAM), acrylic acid (AA, ≥99%), and TA were obtained from the Energy Chemical Co., Ltd. (China). EDTA iron(III) sodium salt (NaFeEDTA) was provided by Anhui Senrise Technology Co., Ltd. *N*,*N*-Methylenebisacrylamide (Bis) and ammonium persulfate (APS, 99%) were purchased from the Sigma-Aldrich Co., Ltd. (USA). The Calcein-AM staining kit for bacteria was supplied by the Biyuntian Biotechnology Company. *Escherichia coli* and *Staphylococcus aureus* were purchased from Lu Wei Science and Technology Co., Ltd. (Shanghai). NIPAM was recrystallized twice from benzene/hexane (v/v, 1/10). Other chemical reagents were used directly without any treatment.

2.2. Preparation of Hydrogel. NIPAM (0.4 g, 3.5 mmol) and AA (1.0 g, 13.8 mmol) were added to deionized water (DI, 4 mL), and the mixture was stirred continuously for 10 min at room temperature to dissolution. Then, *N*,*N*′-methylenebisacrylamide (Bis, 0.012 g, 0.08 mmol) was added to the mixed solution and stirred for 5 min. The completely dissolved prepolymer solution was placed in an ice−water bath under nitrogen for 20 min to remove air bubbles. APS (0.02 g, 0.08 mmol) was quickly added to the solution as the initiator. The resulting solution was poured into the cylindrical glass mold and sealed at 70 °C for 2 h to form hydrogel. Finally, the hydrogel was washed with DI to remove unreacted residues and monomers to obtain hydrogel PNA. PNAF hydrogel was obtained by treating the PNA hydrogel in Fe^{3+} solution (0.03 mol/L) for 15 min. NIPAM, AA, and TA (0.06 g, 0.32 mmol) were added to DI, and the other preparation procedures were the same as that of hydrogel PNA to obtain hydrogel PNAT. The PNATF hydrogel can be obtained after leaving PNAT hydrogel into Fe^{3+} solution for 15 min.

2.3. Characterization. The inter-reactions among AA, TA, and Fe^{3+} were confirmed using a UV−vis spectrophotometer (UV, JASCO, V-630). The chemical structures of different hydrogel samples were analyzed by using a Fourier transform infrared spectrometer (FT-IR, Nicolet 6700, Thermo Elemental). The scanning step was set at 1 cm^{-1}, and the wavelength range was 200−600 cm^{-1}. In addition, the hydrogen structure was observed by a scanning electron microscope (SEM, JSM-6490LV, Hitachi, Ltd.) at an accelerating voltage of 15 keV. Before observation, samples were brittle fractured with liquid nitrogen and treated under vacuum for 24 h. The cross section was sprayed with gold for 45 s.

2.4. Mechanical Tests. All mechanical properties of hydrogels were characterized at room temperature by a universal tensile machine (E42, MTS) with the different parameters as follows. Uniaxial tensile tests were performed at a tensile speed of 5 mm/s, and the dimensions of samples were 20 mm (length) × 4 mm (width). The speed of cyclic loading−unloading tensile tests and compression tests was kept at 50 and 5 mm/min, respectively. The Young's modulus (E) was equated to the slope of the stress−strain curve in the 5−15% strain range, while the toughness (T) was obtained by integrating the area under the stress−strain curve. The final result of each test is the average of at least three repetitions.

2.5. Adhesion and Self-Healing Tests. The adhesion performance of hydrogels with various substrates was represented by the ratio of the maximum load to the bonding area. The contact area of all substrates was set at 1 cm^2, including plastic, aluminum, iron, copper, glass, wood, and rubber.

Three rheological characterization tests were recorded on a rheometer (RH20, Bosin Tech) at room temperature. First, the energy storage modulus (G') and loss modulus (G'') were measured by strain amplitude sweep test from 1 to 100% strain. Next, the hydrogels were scanned with alternating strains of 1 and 200% at a frequency of 1 Hz, with each strain level maintained for 100 s. Then, the hydrogels were subjected to time-scanning tests at a 1% constant strain and 1 Hz constant frequency. Finally, the time-scanning test was performed again on the hydrogel after it was cut into two pieces and self-healed. To quantitatively assess the hydrogels' self-repairing capability after different healing durations, we utilized the self-repairing efficacy (HE, %). Utilizing the aforementioned universal testing machine, the tensile fracture strength of the self-healing hydrogel was assessed at a stretching rate of 50 mm/min. The self-healing capability of the hydrogel following various healing durations was quantitatively gauged via the self-healing efficiency. HE can be calculated as follows:

$$\mathrm{HE} = \frac{S_h}{S_0} \times 100\% \tag{1}$$

where S_h and S_0 represent the signifies the tensile strain at fracture of the hydrogel subsequent to self-healing and the tensile strain at fracture of the pristine hydrogel, respectively.

2.6. Temperature-Responsive Conductivity Tests. The relationship between the conductivity of the sample and the response to temperature was determined by a sandwich structure temperature sensor, which was prepared by connecting a rectangular hydrogel (50 mm × 10 mm × 3 mm) to conductive copper tape and wires at both ends and sealing the hydrogel surface with tape. During the experiment, the temperature sensor was placed in a benchtop thermostat (SH-261, ESPEC, Germany) and connected to an electrochemical workstation (CHI 760E) by wires. The impedance of the sensor in the open circuit state was monitored with the electrochemical workstation by changing the thermostat's temperature from 20 to 60 °C at a rate of 5 °C/min. The resistance (R) can be calculated as follows:

$$R = \frac{U}{I} \tag{2}$$

where U and I represent the real-time voltage and current, respectively.

The relative resistance change rate $\Delta R/R_0$ can be obtained as the following formula:

$$\frac{\Delta R}{R_0} = \frac{R - R_0}{R_0} \tag{3}$$

where R and R_0 represent the real-time resistance and the original resistance.

2.7. pH-Responsive Conductivity Tests. The relationship between the conductivity of the sample and the response to pH was determined by a pH sensor, which was prepared by connecting a rectangular hydrogel (50 × 10 × 3 mm) to conductive copper tape and wires at both ends. During the experiment, the pH sensor was immersed in the PBS solution and connected to an electrochemical workstation (CHI 760E) by wires. The impedance of the sensor in the open-circuit state was monitored by the electrochemical workstation while obtaining different pH values by changing the composition of the PBS solution. The final result is the average of at least three repetitions.

2.8. Water Retention Tests. The hydrogel was prepared as a circular disc with a diameter of 20 mm and a thickness of 4 mm. The weights were carried out at different times at 25 and 37 °C with 40% humidity. The weight ratio can be calculated as follows:

$$\text{weight ratio}(\%) = \frac{W_0 - W_t}{W_0} \times 100\% \tag{4}$$

where W_t and W_0 represent the hydrogel mass at different times and the initial mass, respectively.

2.9. Strain-Responsive Conductivity Tests. The relationship between the conductivity of the sample and the response to strain was determined by connecting a rectangular hydrogel to conductive copper strips at both ends, and the copper strips were connected to an electrochemical workstation (CHI 760E). The relative resistance change rate ($\Delta R/R_0$) of the hydrogel was monitored by the electrochemical workstation while subjected to different strains by a universal tensile testing machine.

3. RESULTS AND DISCUSSION

3.1. Structural Characterization. In the UV−visible spectroscopy analysis of the PNATF hydrogel (Figure 1a),

https://doi.org/10.1021/acsapm.4c03794
ACS Appl. Polym. Mater. 2025, 7, 2529−2540

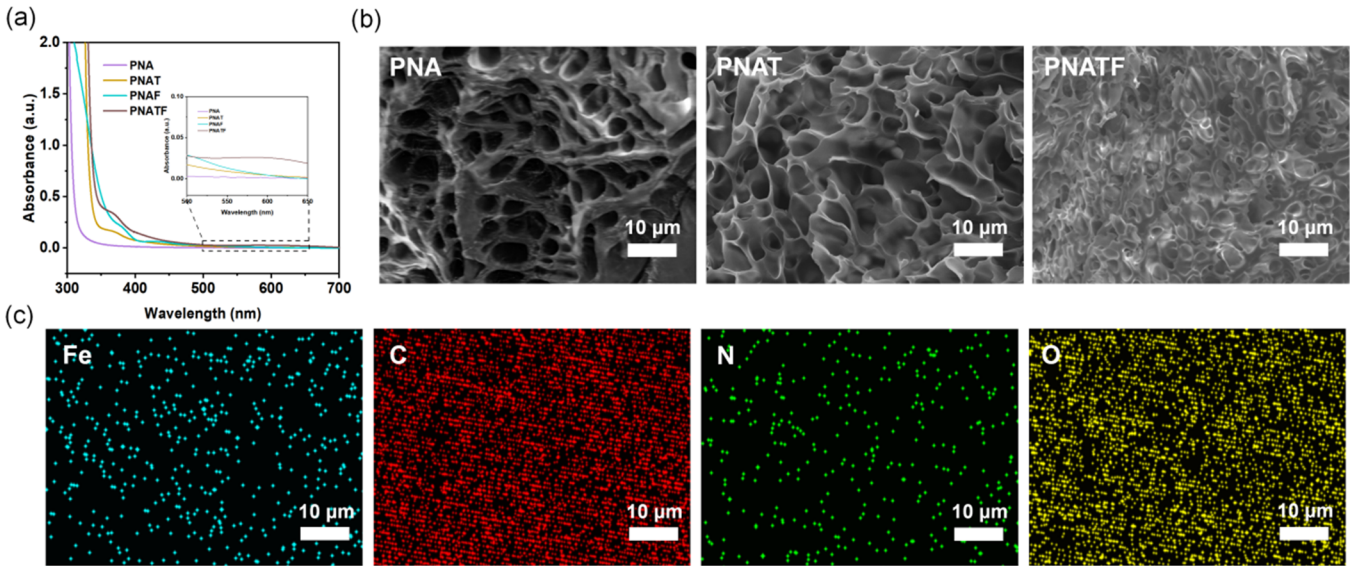

Figure 1. Structural characterization of PNATF hydrogels. (a) UV−vis spectra. (b) SEM images of PNA, PNAT, and PNATF hydrogels. (c) Elemental mapping of PNATF hydrogels.

the spectrum revealed a distinct gap between the PNA hydrogel and the PNAT hydrogel, indicating the successful incorporation of TA into the hydrogel matrix. Since neither pure AA nor Fe^{3+} displays absorbance, the detectable absorbance in the PNATF hydrogel suggests the formation of a coordination bond between AA and Fe^{3+}. Furthermore, the peak at 560 nm confirms the successful construction of the metal−catechol bond between TA and Fe^{3+}.[53] The FTIR spectra (Figure S1) show that 1385 and 1366 cm^{-1} are the isopropyl peaks of NIPAM, and 1650 and 1450 cm^{-1} are the characteristic peaks of C═O and C−O of AA. 672 and 572 cm^{-1} are the C−H bending vibrations of TA, proving the successful introduction of TA. 610 cm^{-1} is the tensile vibration peak of the Fe−O bond,[54] indicating an ionic cross-link between the carboxyl group of AA and Fe^{3+}. With Fe^{3+} incorporation, the −OH vibration of TA decreases from 3442 to 3428 cm^{-1}.

All SEM images of different samples (PNA, PNAT, and PNATF hydrogels) are shown in Figure 1b. Interconnected porous network structures were observed in all the hydrogel samples, which facilitates the free diffusion of water molecules. As can be seen from the diagram, the pore structure becomes more compact with the gradual introduction of catechol (−OH), carboxyl (−COOH), and Fe^{3+}. It is attributed to the introduced functional groups and ions that promote the formation of dynamic hydrogen bonds, complexation, and ionic interactions, thereby increasing the cross-linking density of the hydrogels. The uniform distribution of C, O, N, and Fe elements within the hydrogel can be observed from the elemental mapping results (Figure 1c), which contributes to the enhanced mechanical strength of the hydrogel.[55]

3.2. Mechanical Properties. The different mechanical properties of hydrogels have been investigated, as shown in Figure 2. The superior strength and toughness of the hydrogels are demonstrated in Figure 2a, and it can be manually stretched to different lengths within the tensile limit without any damage after being twisted and knotted. Additionally, the prominent load-bearing capacity and reversibility of the hydrogel during compression and relaxation processes can be seen in Figure 2b. As shown in Figure S2, the fracture elongation of the hydrogel containing Na^+/Fe^{3+} is up to 2320%, which is 1.5 and 5.8 times that of containing Na^+ alone (1557%) and Fe^{3+} alone (402%), respectively. Sodium ions enhance the tensile ability of hydrogels by affecting hydration. Sodium ions interact with water molecules to form a hydration shell, which affects the dynamic characteristics of water molecules and produces different osmotic pressures, so that salt ions diffuse into the hydrogel, and at the same time capture water molecules in the hydration layer of the polymer to promote the hydrogen bond between polymer chains.[56,57] Iron ions, by complexing with functional groups, excessively cross-link and thus limit the stretching capacity. The iron ions provided by NaFeEDTA showed more uniform and stable binding during coordination than iron ions provided by $FeCl_3$.

In order to further assess the mechanical properties, uniaxial tensile and compression tests were performed on the hydrogels with different compositions (Figure 2c,d). It can be seen that the fracture elongation increases with the addition of components; the optimum fracture elongation is 2630% of the PNATF hydrogel.[58] It can be attributed to the coordination between Fe^{3+} and catechols as well as carboxyl groups, which can serve as cross-linking points to enhance the mechanical properties of the hydrogel. Compared with PNATF and PNAT hydrogels, PNA hydrogels showed the highest Young's modulus. PNATF hydrogels, when immersed in an Fe^{3+} ionic solution, experience network expansion. This expansion increases the distance between the cross-links in the network, thereby reducing the material's rigidity.[59,60] The introduction of TA in PNAT hydrogels increases the number of flexible chain segments in the hydrogel network. These segments are more likely to deform under stress, thus reducing the Young's modulus of the material.[61] Meanwhile, the addition of Fe^{3+} content will also lead to an increase in the compressive modulus of the hydrogel.[62]

Figure 2e displays the loading−unloading curves of hydrogels at different strains. Obvious hysteresis can be observed in the graph after unloading under different conditions, which demonstrates that the hydrogels effectively dissipate energy under stretching. Subsequently, five consecutive loading−unloading cycles were conducted on the hydrogels to further

https://doi.org/10.1021/acsapm.4c03794
ACS Appl. Polym. Mater. 2025, 7, 2529−2540

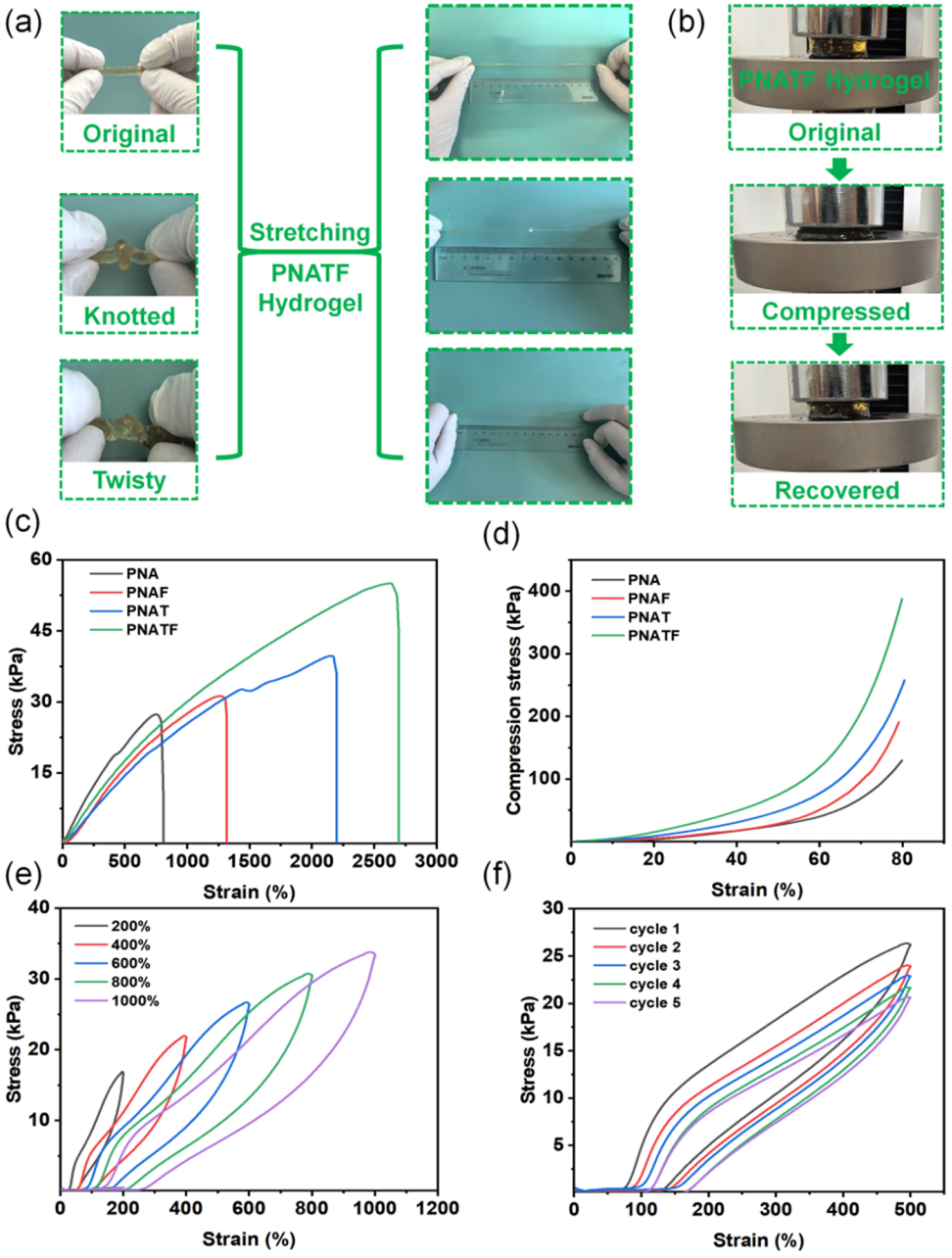

Figure 2. Mechanical properties of the PNATF hydrogels. Photographs of the PNATF hydrogel under (a) stretching and (b) compressing. (c) Tensile stress−strain curves and (d) compression stress−strain curves of hydrogels with different components. (e) Stress−strain curves of the PNATF hydrogel for a loading−unloading tensile cycle under varied strain at a speed of 50 mm/min. (f) Cyclic loading−unloading tensile tests of the PNATF hydrogel under 500% strain at a speed of 50 mm/min.

evaluate the strain recovery. As shown in Figure 2f, the phenomenon of the hydrogel rapidly recovering to its initial condition after each cycle demonstrates its excellent fatigue resistance. The superior comprehensive mechanical properties of the hydrogels are mainly due to the formation of dynamic hydrogen bonding, coordination bonding, and ionic bonds between −OH, −COOH, and Fe^{3+} within the network, in which dissociation and reorganization can provide efficient energy dissipation.

3.3. Adhesion and Self-Healing Stability. The adhesion strength between hydrogels and different surfaces is crucial for their application in wearable devices. As shown in Figure 3a−d, the strong adhesion strength of PNATF hydrogel with various materials (glass, wood, rubber, metal, and plastic) has been verified. The adhesion strengths of hydrogel with glass, wood, metal, skin, plastic, and rubber are 3.96, 12, 4.15, 7.06, 10.36, and 5.64 kPa, respectively. It is attributed to the $p-\pi$ conjugation between the benzene ring and the oxygen atom in TA and increased polarity of the catechol moiety.[63] Additionally, the dynamic adhesion and peel test between the hydrogel and the skin was also investigated (Figure 3e,f). It can be confirmed that the hydrogel can maintain seamless and stable adhesion with skin during the dynamic bonding process and at the same time ensure no residue when peeling off.

The self-healing performance of hydrogels can be characterized by a continuous step strain method. As depicted in Figure 3g, the critical strain for PNATF hydrogel is approximately 120%, and the G' (storage modulus) of the

https://doi.org/10.1021/acsapm.4c03794
ACS Appl. Polym. Mater. 2025, 7, 2529−2540

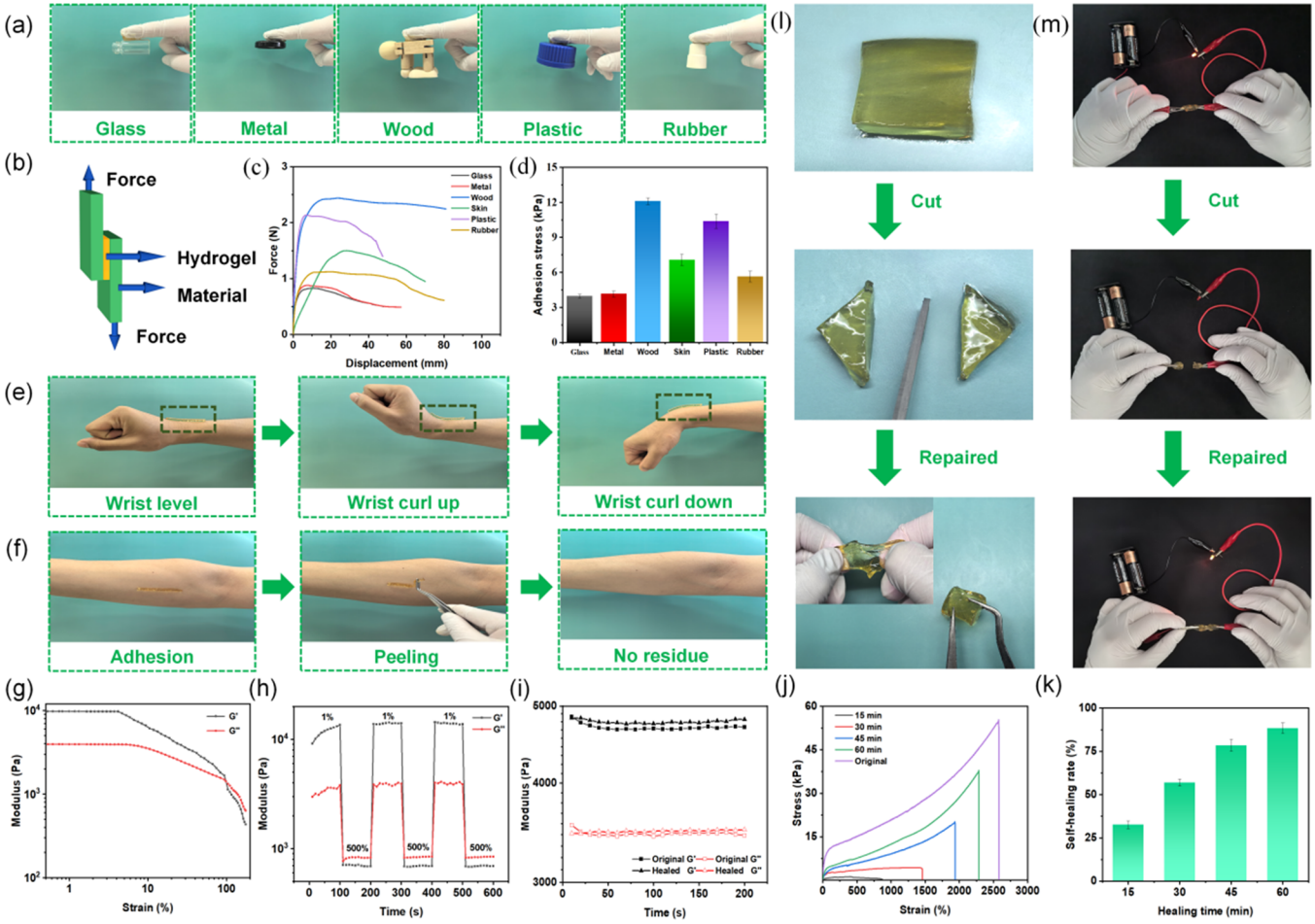

Figure 3. Adhesive properties and self-healing of PNATF hydrogels. (a) Photographs of the hydrogel adhered to various surfaces, including wood, plastic, glass, rubber, and aluminum. (b) Schematic diagram and digital photograph of shear adhesion. Instantaneous adhesion (c) strength–displacement curve and (d) adhesion strength. (e) No residue is observed during the process of peeling from the arm skin. (f) The hydrogel is seamlessly contacted with a nonplanar skin under dynamic movement. (g) The strain amplitude sweep test of hydrogels. (h) Alternate step strain sweep test with small strain (1.0%) to subsequent large strain (500%) with 100 s for every strain interval. (i) Storage modulus and loss modulus of original hydrogel and healed hydrogel profile. (j) Self-healing rates of the PNATF hydrogel at different times. (k) HE of the PNATF hydrogel at different healing times. (l) Photographs of self-healing behavior of the hydrogel with mechanical damage. (m) Photographs and illustration of self-healing behavior of the hydrogel for designed circuit.

hydrogel is higher than G'' (loss modulus) when the strain is lower than 120%, and G' is lower than G'' when the strain is higher than 120%. This indicates that the hydrogel structure is completely broken when the strain is greater than 120%. Then, the hydrogel was subjected to cyclic strains of 500 and 1%. The value of G' is lower than that of G'' at 500% strain, which indicates the destruction of the network structure. However, G' immediately becomes larger than G'' when the strain is brought back to 1%, which indicates that the collapse and recovery of the hydrogel is repeatable (Figure 3h). The storage modulus and loss modulus of the hydrogel before and after repair shown in Figure 3i are almost the same, which also confirms the self-healing property of the hydrogel. In order to characterize the self-healing property more intuitively, we tested the macroscopic behavior of the hydrogels was tested. In addition, the self-healing efficiency of the PNATF hydrogel was examined. Figure 3j and 3k illustrate the tensile curves of the original PNATF hydrogel and the hydrogel after different self-healing times, respectively. The results showed that the elongation at break of the healed hydrogel gradually increased with the extension of the self-healing time. At the same time, the self-healing efficiency of the hydrogel was calculated based on the ratio of the break length of the self-healing hydrogel to the original hydrogel. The results showed that the self-healing efficiency of PNATF hydrogel was 88.06% after 60 min of self-healing. It can be seen from Figure 3l that the hydrogel separated into two segments can complete healing after contact at room temperature, and the fracture boundary will become blurred.

Finally, the self-healing ability of the hydrogel was also demonstrated by constructing a circuit consisting of an LED bulb, two 1.5 V batteries, and a PNATF hydrogel (Figure 3m). The LED can be successfully lit by the hydrogel connected to the circuit; as the hydrogel is cut and healed, the small light will turn off and relight in sequence. This self-healing capability is primarily attributed to the rapid formation and reconstruction of dynamic bonds between Fe^{3+}, phenol groups, and carboxyl groups at the contact surface. It can be inferred that the hydrogels can be applied in more extreme and harsh conditions depending on their excellent self-healing property.

3.4. Temperature and pH-Responsive Conductivity Properties. The light transmission performance of hydrogels

https://doi.org/10.1021/acsapm.4c03794
ACS Appl. Polym. Mater. 2025, 7, 2529−2540

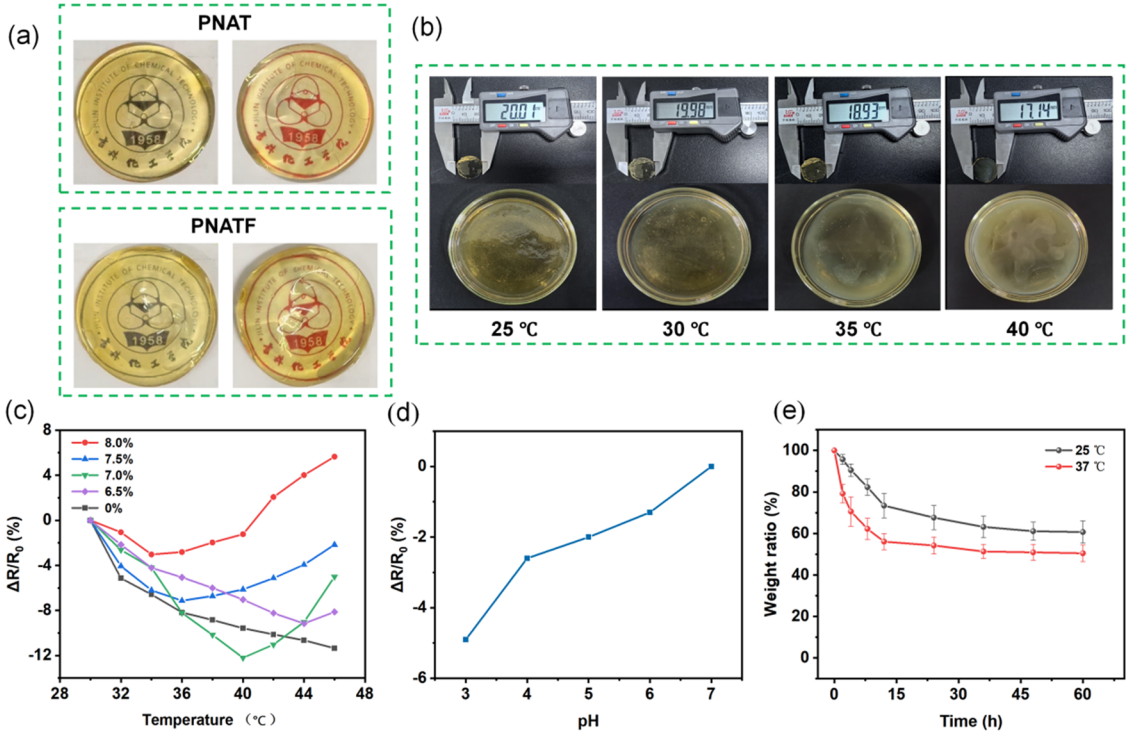

Figure 4. (a) Transparency of PNAT and PNATF hydrogels. (b) PNATF hydrogel with different temperatures. (c) Relative impedance change ($\Delta R/R_0$)−temperature curves of PNATF hydrogels with different NIPAM mass fractions. (d) Relative impedance change ($\Delta R/R_0$)−pH curve of the pH-responsive PNATF hydrogel. (e) Water retention of the PNATF hydrogel at different temperatures.

is shown in Figure 4a. The scenery can be seen clearly through the hydrogels depending on their excellent optical properties. The excellent field-of-view clarity is conducive to rapid identification and localization of potential issues.

With the introduction of NIPAM, the hydrogel showed a good temperature sensitivity. Figure 4b illustrates the phase transition change of the PNAFT hydrogel with increasing ambient temperature. At the same time, the phase separation process of the hydrogel is significantly hygroscopic, which can be analyzed by differential scanning calorimetry (DSC), and the exothermic peak of the curve is the critical solution temperature (LCST) of the hydrogel. The absorption peak values of the curves are shown in Figure S3 for the DSC curves of PNATF hydrogels with different NIPAM mass fractions. The LCST of the hydrogel can be modulated by the copolymerization reaction of AA and NIPAM. The DSC curve of the hydrogel showed that the LCST temperatures of the hydrogel with NIPAM mass fraction of 8, 7.5, 7, and 6.5% were 37.5, 38.2, 39.9, and 41.6 °C, respectively. The phase transition temperature of the hydrogel increased to 41.6 °C with an increasing AA content. Therefore, adjusting the raw material concentration can prepare hydrogels suitable for the operating temperature range of the flexible sensor, showing specific LCST values.[64] Based on these findings, we further explored the thermosensitive properties of hydrogels as temperature sensors. The relative impedance ($\Delta R/R_0$) of the hydrogel sensors with different mass fractions of NIPAM is summarized in Figure 4c. With the incorporation of NIPAM and AA, the $\Delta R/R_0-T$ curve of the sensor changed from a linear without a turnaround point to a V-shaped with a turnaround point, which indicated the existence of temperature responsiveness. The turnaround point corresponding to the lower critical solution temperature (LCST). Previous studies have shown that the phase transition temperature of PNIPAM hydrogels is 32 °C, which is increased by copolymerization with other hydrophilic monomers. The addition of AA introduces the carboxyl group of the hydrophilic group, and with the increase of AA content, this hydrophilic effect is enhanced, which causes the original hydrophilic and hydrophobic balance to change, leading to the increase of the phase transition point temperature.[65] Notably, this indicates significant potential for the hydrogel material in real-time monitoring of ambient temperatures and detection of changes in human body temperatures, such as fever symptoms.

Meanwhile, the introduction of AA monomers also endowed the hydrogels with excellent pH sensitivity. The variation of the relative impedance rate at different pH values is shown in Figure 4d. Upon exposure to a PBS solution, the resistance of the hydrogel decreased as the pH value increased. We believe that this is due to the interaction between the hydrogel and the ions; AA contains carboxyl (−COOH) functional groups, which will exhibit different ionization states at different pH values. With increasing pH, the carboxyl group gradually loses protons (H^+) and turns into a negative ion (COO^-). The ionization process increases the concentration of free ions in the hydrogel, which improves its ionic conductivity and leads to a decrease in the relative resistance. Simultaneously, the ionization of carboxyl groups results in an increase in negative ion concentration, causing the hydrogel network to swell and enhancing ion mobility.[66] The phenomena can facilitate various potential applications, particularly in monitoring pH changes caused by sweat during physical activity.

3.5. Water Retention Properties. Next, the water retention properties of the PNATF hydrogels were evaluated. In the water retention test, the solid content of the hydrogel at different temperatures remained consistent. The water

https://doi.org/10.1021/acsapm.4c03794
ACS Appl. Polym. Mater. 2025, 7, 2529−2540

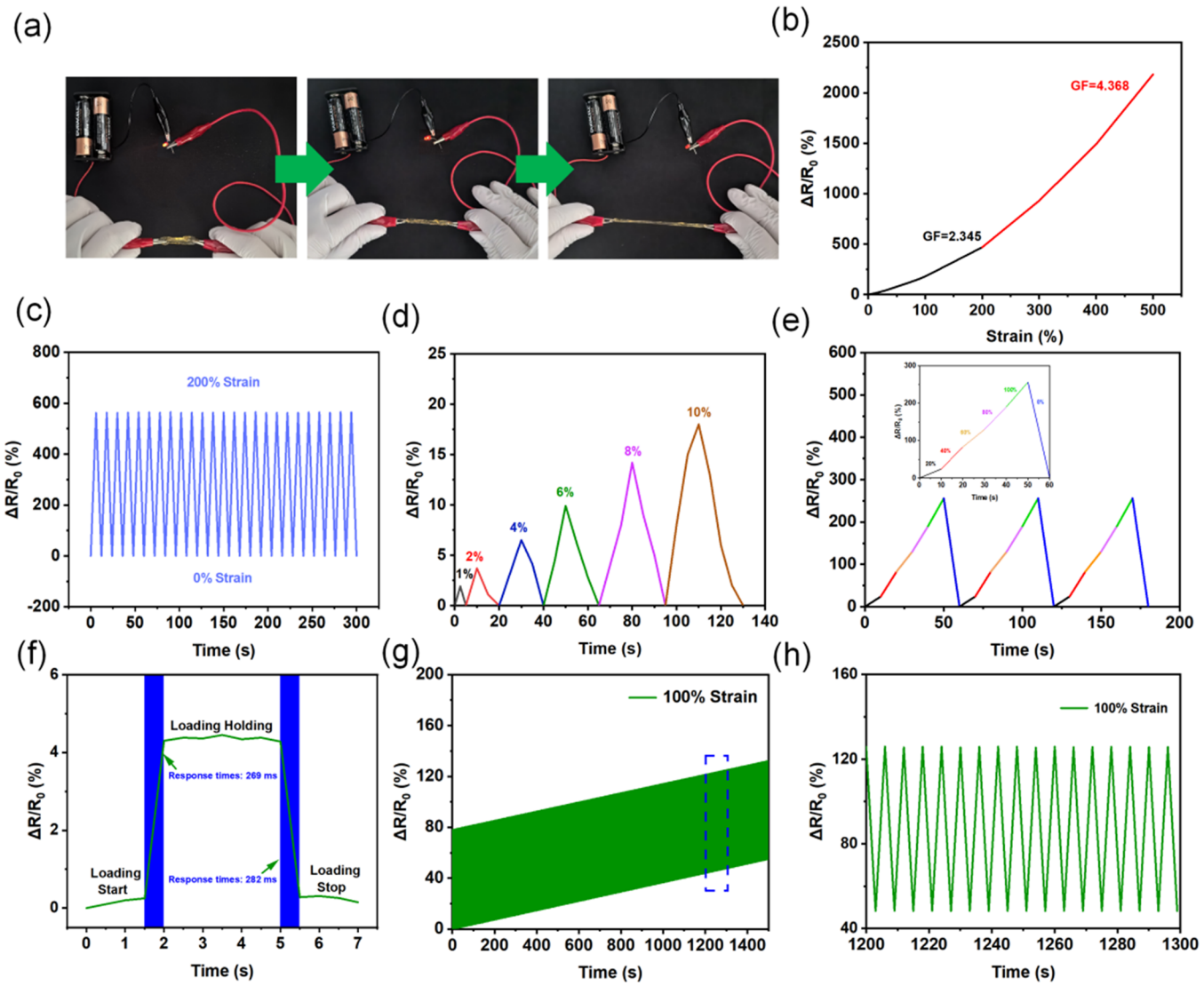

Figure 5. Conductive behaviors of PNATF hydrogels. (a) Luminance variation in an LED bulb with the stretching of the hydrogel. (b) Relative resistance changes ($\Delta R/R_0$)−strain curve of the hydrogel and the corresponding strain sensitivity factor (GF). (c) $\Delta R/R_0$ of hydrogel during cyclic loading/unloading tests with strain varying between 0 and 200%. (d) $\Delta R/R_0$ of the hydrogel under low strain (less than 10%) stretching cycles. (e) $\Delta R/R_0$ of the hydrogel during cyclic loading/unloading tests with strain varying between 0 and 100%. The inset figure is the enlarged view of $\Delta R/R_0$ during one cycle. (f) Response time and recovery time of hydrogel under loading and unloading stretching. (g) Electrical cycle stability of hydrogel during the 500 consecutive cycles under 100% strain and (h) its detailed diagram from 1200 to 1300 s.

retention test (25 °C, 37 °C, and 40% RH) showed that the water retention of the PNATF hydrogel was 60.08% at 25 °C and 51.9% at 37 °C (Figure 4e). This can be attributed to the formation of hydrogen bonds between hydrophilic groups and water molecules, thereby enhancing the water retention ability of the hydrogel.

3.6. Strain-Responsive Conductivity Properties. The strain-responsive conductivity property of the hydrogel was demonstrated by constructing a circuit consisting of an LED bulb, two 1.5 V batteries, and a PNATF hydrogel (Figure 5a). The experiments show that the brightness of the LED becomes darker with the increase of hydrogel strain and brighter with the decrease of strain, confirming the instantaneous response of the PNATF hydrogel to strain. Figure S4 shows that the hydrogel immersed in the NaFeEDTA solution has the highest electrical conductivity. Figure S5 reveals the positive correlation between Fe^{3+} content and ionic conductivity of the hydrogel, and the hydrogel's conductivity reaches 1.28 S·m^{-1} when Fe^{3+} is 0.03 mol/L.

Furthermore, the strain-responsive sensitivity of the PNATF hydrogel was evaluated by measuring the relative resistance change rate ($\Delta R/R_0$) of the hydrogel at different strains. As shown in Figure 5b, $\Delta R/R_0$ increased almost linearly with increasing tensile strain from 0 to 500% with a measurement factor (GF) that increased slowly and uniformly. The GF of the PNATF hydrogel at 200% strain was 2.345, and when the strain is increased to 500%, the GF increases to 4.368, indicating the high sensitivity of the hydrogel over a large strain range. Compared with the reported representative hydrogel strain sensors, the GF value of our hydrogel was high.[67,68] The stability of the response is shown in Figure 5c−h5

3.7. Sensors for the Monitoring of Human Sweating, Fever, and Movement. Continuous monitoring of physiological parameters during human body movements can be

https://doi.org/10.1021/acsapm.4c03794
ACS Appl. Polym. Mater. 2025, 7, 2529−2540

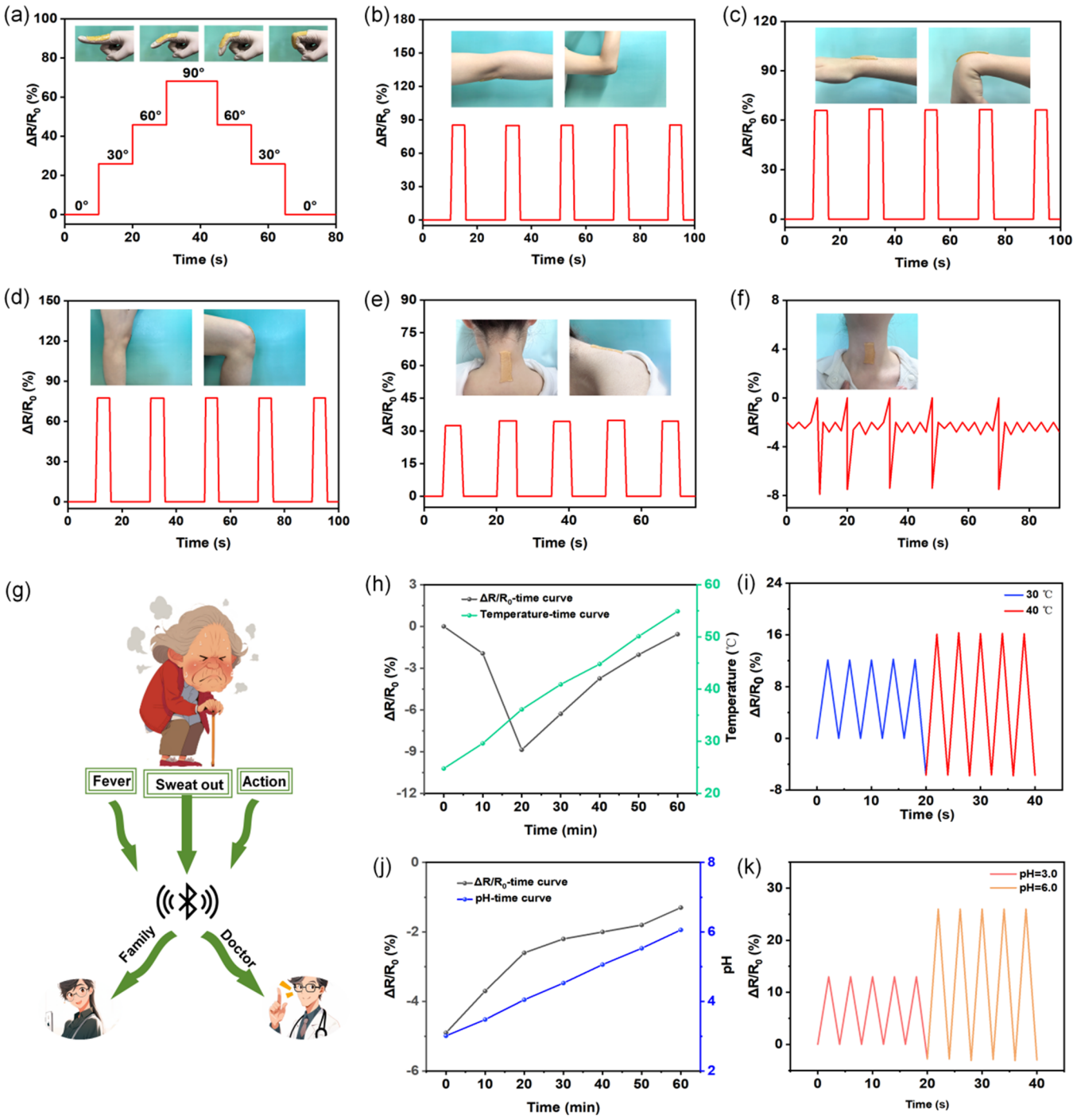

Figure 6. (a) Relative variations in resistance of hydrogel sensors when fingers are bent at different angles (0, 30, 60, and 90°). The relative variations in resistance of the hydrogel in response to human motions: (b) elbow, (c) wrist, (d) knee, (e) neck joint bent and release, and (f) swallowing. (g) Picture of doctors and family members detecting illness in the elderly through abnormal signals transmitted by skin temperature, pH, and body movements. (h) Resistance curve of hydrogel at different temperatures. (i) Resistance curve of 50% strain after stretching−recovery at different temperatures. (j) Resistance curve of hydrogel at different pH. (k) Resistance curve of 50% strain after stretching−recovery at different pH.

achieved by assembling the PNATF hydrogel into a sensor connected to a computer. As shown in Figure 6a, the sensor was able to distinguish the resistance change of the finger under different bending degrees (0, 30, 60, and 90°) and maintain the stability of the resistance at a specific angle, proving superior reliability of the sensor. Moreover, they maintain electrical signal transmission during vigorous or repetitive movements. In addition, the hydrogel sensor can be employed as a motion sensor to detect and distinguish macroscopic limb movements, including elbow, wrist, knee, and cervical vertebrae, as illustrated in Figure 6b−6e. Moreover, effective electrical signal transmission will be maintained even during vigorous or repetitive movements. Furthermore, the hydrogel sensors also show rapid, stable, and highly repeatable response characteristics to small-amplitude motions such as swallowing. These features indicate that

https://doi.org/10.1021/acsapm.4c03794
ACS Appl. Polym. Mater. 2025, 7, 2529−2540

hydrogel sensors have significant potential for applications in behavioral monitoring and personal health assessment.

In order to investigate the potential application of hydrogel sensors in detecting physiological signal changes, the sensing ability of hydrogels in a fever state was simulated and its response under small strains was simulated, as illustrated in Figure 6g–i. The hydrogel exhibited stable and different electrical output signals at various temperatures under 50% tensile strain. Apart from temperature, the hydrogel can also produce stable electrical signal outputs at different pH values under 50% tensile strain (Figure 6k,j), allowing for continuous and real-time temperature and pH monitoring with enhanced accuracy and convenience.

4. CONCLUSIONS

In summary, PNATF transparent ionic conductivity hydrogels with interwoven network structures were successfully prepared by incorporating ligands. It can be inferred that the excellent mechanical properties and fast self-healing ability are attributed to the cross-linking of Fe^{3+} with TA, including ultrahigh stretchability of 2638%, strength of 355 kPa, and skin adhesion of 7.06 kPa. The Na^{+} and Fe^{3+} contained in the ligand conferred and enhanced the conductivity of the hydrogel (1.28 $S{\cdot}m^{-1}$). The possibility of the hydrogel as a wearable sensor was demonstrated by separately investigating its responsiveness to pH, temperature, and strain. The PNATF ionic conductivity hydrogels exhibit a stable and rapid response of 265 ms during human movements. In addition, the critical phase transition temperature of 37 °C enables it to monitor fluctuations in human temperature with real-time monitoring. At the same time, it can also respond to pH changes caused by sweat secretion during exercise. The ionic conductive hydrogel designed in this study will have great application potential as a temperature-sensitive sensor in monitoring human movement, which also provides a unique perspective for combining conductive materials with stimulus-responsive hydrogels.

■ ASSOCIATED CONTENT

Data Availability Statement

The authors do not have permission to share data.

Supporting Information

The Supporting Information is available free of charge at https://pubs.acs.org/doi/10.1021/acsapm.4c03794.

FTIR spectra of hydrogels (Figure S1); stress–strain curves of the hydrogels immersed in Na^{+}, Fe^{3+}, and Na^{+}/Fe^{3+} solutions (Figure S2); DSC curves of PNATF hydrogels with different NIPAM mass fractions (Figure S3); ionic conductivities of the hydrogels immersed in Na^{+}, Fe^{3+}, and Na+/Fe^{3+} solutions (Figure S4); and ionic conductivities of the hydrogels with different concentration of Fe^{3+} (Figure S5) (PDF)

■ AUTHOR INFORMATION

Corresponding Authors

Hong Yu Yang − *College of Materials Science and Engineering, Jilin Institute of Chemical Technology, Jilin City, Jilin Province 132022, China*; orcid.org/0000-0002-0730-2779; Email: yanghy@jlict.edu.cn

Changling Liu − *College of Materials Science and Engineering, Jilin Institute of Chemical Technology, Jilin City, Jilin Province 132022, China*; Email: liuchangling@jlict.edu.cn

Authors

Yan Liu − *College of Materials Science and Engineering, Jilin Institute of Chemical Technology, Jilin City, Jilin Province 132022, China*

Yirong Wang − *College of Chemistry and Pharmaceutical Engineering, Jilin Institute of Chemical Technology, Jilin City, Jilin Province 132022, China*

Yan Fu − *College of Materials Science and Engineering, Jilin Institute of Chemical Technology, Jilin City, Jilin Province 132022, China*

Nan Nan Wang − *College of Biology & Food Engineering, Jilin Institute of Chemical Technology, Jilin, Jilin Province 132022, China*

Si Qi Zhan − *College of Materials Science and Engineering, Jilin Institute of Chemical Technology, Jilin City, Jilin Province 132022, China*

Li Sheng − *College of Materials Science and Engineering, Jilin Institute of Chemical Technology, Jilin City, Jilin Province 132022, China*

Complete contact information is available at: https://pubs.acs.org/10.1021/acsapm.4c03794

Author Contributions

[1]Y.L. and Y.W. contributed equally to this paper.

Author Contributions

Yan Liu: writing—review and editing, writing—original draft, methodology, and investigation. Yirong Wang: writing—original draft, methodology, and investigation. Yan Fu: writing—original draft, methodology, and investigation. Nan Nan Wang: writing—original draft, methodology, and investigation. Si Qi Zhan: writing—original draft, methodology, and investigation. Li Sheng: writing—original draft, methodology, and investigation. Hong Yu Yang: writing—review and editing, supervision, project administration, funding acquisition, and conceptualization. Changling Liu: writing—review and editing, supervision, project administration, funding acquisition, and conceptualization.

Notes

The authors declare no competing financial interest.

■ ACKNOWLEDGMENTS

This work was supported by the Scientific Research Project of Education Department of Jilin Province (JJKH20230297KJ, JJKH20241768KJ, and JJKH20200245KJ) and Natural Science Foundation of Jilin Province (20240101099JC). The authors acknowledge the assistance of JLICT Center of Analysis Characterization and Analysis.

■ REFERENCES

(1) Liu, Y.; Pharr, M.; Salvatore, G. A. Lab-on-skin: a review of flexible and stretchable electronics for wearable health monitoring. *ACS Nano* **2017**, *11* (10), 9614–9635.

(2) Ray, T. R.; Choi, J.; Bandodkar, A. J.; Krishnan, S.; Gutruf, P.; Tian, L.; Ghaffari, R.; Rogers, J. A. Bio-integrated wearable systems: a comprehensive review. *Chem. Rev.* **2019**, *119* (8), 5461–5533.

(3) Teymourian, H.; Parrilla, M.; Sempionatto, J. R.; Montiel, N. F.; Barfidokht, A.; Van Echelpoel, R.; Wang, J. Wearable electrochemical sensors for the monitoring and screening of drugs. *ACS Sens.* **2020**, *5* (9), 2679–2700.

(4) Huang, S.; Liu, Y.; Zhao, Y.; Ren, Z.; Guo, C. F. Flexible electronics: stretchable electrodes and their future. *Adv. Funct. Mater.* **2019**, *29* (6), No. 1805924.

(5) Wang, P.; Hu, M.; Wang, H.; Chen, Z.; Feng, Y.; Wang, J.; Ling, W.; Huang, Y. The evolution of flexible electronics: from nature, beyond nature, and to nature. *Adv. Sci.* **2020**, *7* (20), No. 2001116.
(6) Wang, Z.; Cong, Y.; Fu, J. Stretchable and tough conductive hydrogels for flexible pressure and strain sensors. *Mater. Chem. B* **2020**, *8* (16), 3437−3459.
(7) Yuk, H.; Lu, B.; Zhao, X. Hydrogel bioelectronics. *Chem. Soc. Rev.* **2019**, *48* (6), 1642−1667.
(8) Zhao, S.; Li, J.; Cao, D.; Zhang, G.; Li, J.; Li, K.; Yang, Y.; Wang, W.; Jin, Y.; Sun, R.; Wong, C. P. Recent advancements in flexible and stretchable electrodes for electromechanical sensors: strategies, materials, and features. *ACS Appl. Mater. & Interfaces.* **2017**, *9* (14), 12147−12164.
(9) Trung, T. Q.; Ramasundaram, S.; Hwang, B. U.; Lee, N. E. An all-elastomeric transparent and stretchable temperature sensor for body-attachable wearable electronics. *Adv. Mater.* **2016**, *28* (3), 502−509.
(10) Zhang, Q.; Liu, X.; Duan, L.; Gao, G. Nucleotide-driven skin-attachable hydrogels toward visual human-machine interfaces. *J. Mater. Chem. A* **2020**, *8* (8), 4515−4523.
(11) Wang, Y.; Hao, J.; Huang, Z.; Dai, K.; Liu, C.; Shen, C. Flexible electrically resistive-type strain sensors based on reduced graphene oxide-decorated electrospun polymer fibrous mats for human motion monitoring. *Carbon.* **2018**, *126*, 360−371.
(12) Chen, G.; Wang, H.; Guo, R.; Duan, M.; Zhang, Y.; Liu, J. Superelastic EGaIn composite fibers sustaining 500% tensile strain with superior electrical conductivity for wearable electronics. *ACS Appl. Mater. Interfaces.* **2020**, *12* (5), 6112−6118.
(13) Choi, Y. Y.; Ho, D. H.; Cho, J. H. Self-healable hydrogel−liquid metal composite platform enabled by a 3D printed stamp for a multimodular sensor system. *ACS Appl. Mater. Interfaces* **2020**, *12* (8), 9824−9832.
(14) Lu, Y.; Yue, Y.; Ding, Q.; Mei, C.; Xu, X.; Wu, Q.; Xiao, H.; Han, J. Self-recovery, fatigue-resistant, and multifunctional sensor assembled by a nanocellulose/carbon nanotube nanocomplex-mediated hydrogel. *ACS Appl. Mater. Interfaces.* **2021**, *13* (42), 50281−50297.
(15) Zhu, S.; Lu, Y.; Wang, S.; Sun, H.; Yue, Y.; Xu, X.; Mei, C.; Xiao, H.; Fu, Q.; Han, J. Interface design of stretchable and environment-tolerant strain sensors with hierarchical nanocellulose-supported graphene nanocomplexes. *Compos Part A-Appl. S.* **2023**, *164*, No. 107313.
(16) Han, L.; Lu, X.; Wang, M.; Gan, D.; Deng, W.; Wang, K.; Fang, L.; Liu, K.; Chan, C. W.; Tang, Y.; Weng, L.; Yuan, H. A mussel-inspired conductive, self-adhesive, and self-healable tough hydrogel as cell stimulators and implantable bioelectronics. *Small.* **2017**, *13* (2), 1601916.
(17) Li, L.; Zhang, Y.; Lu, H.; Wang, Y.; Xu, J.; Zhu, J.; Zhang, C.; Liu, T. Cryopolymerization enables anisotropic polyaniline hybrid hydrogels with superelasticity and highly deformation-tolerant electrochemical energy storage. *Nat. Commun.* **2020**, *11* (1), 62.
(18) Chen, J.; Peng, Q.; Thundat, T.; Zeng, H. Stretchable, injectable, and self-healing conductive hydrogel enabled by multiple hydrogen bonding toward wearable electronics. *Chem. Mater.* **2019**, *31* (12), 4553−4563.
(19) Wu, J.; Wu, Z.; Lu, X.; Han, S.; Yang, B. R.; Gui, X.; Tao, K.; Miao, J.; Liu, C. Ultrastretchable and stable strain sensors based on antifreezing and self-healing ionic organohydrogels for human motion monitoring. *ACS Appl. Mater. Interfaces* **2019**, *11* (9), 9405−9414.
(20) Huang, H.; Han, L.; Fu, X.; Wang, Y.; Yang, Z.; Pan, L.; Xu, M. A powder self-healable hydrogel electrolyte for flexible hybrid supercapacitors with high energy density and sustainability. *Small* **2021**, *17* (10), No. 2006807.
(21) Liang, Y.; Wu, Z.; Wei, Y.; Ding, Q.; Zilberman, M.; Tao, K.; Xie, X.; Wu, J. Self-healing, self-adhesive and stable organohydrogel-based stretchable oxygen sensor with high performance at room temperature. *Nanomicro Lett.* **2022**, *14* (1), 52.
(22) Jiang, C.; Lai, X.; Wu, Z.; Li, H.; Zeng, X.; Zhao, Y.; Zhu, Y. A high-thermopower ionic hydrogel for intelligent fire protection. *J. Mater. Chem. A* **2022**, *10* (40), 21368−21378.
(23) Gao, Z.; Kong, L.; Jin, R.; Liu, X.; Hu, W.; Gao, G. Mechanical, adhesive and self-healing ionic liquid hydrogels for electrolytes and flexible strain sensors. *J. Mater. Chem. C* **2020**, *8* (32), 11119−11127.
(24) He, Z.; Yuan, W. Highly stretchable, adhesive ionic liquid-containing nanocomposite hydrogel for self-powered multifunctional strain sensors with temperature tolerance. *ACS Appl. Mater. Interfaces.* **2021**, *13* (44), 53055−53066.
(25) Ding, Y.; Zhang, J.; Chang, L.; Zhang, X.; Liu, H.; Jiang, L. Preparation of high-performance ionogels with excellent transparency, good mechanical strength, and high conductivity. *Adv. Mater.* **2017**, *29* (47), No. 1704253.
(26) Chen, Z.; Liu, J.; Chen, Y.; Zheng, X.; Liu, H.; Li, H. Multiple-stimuli-responsive and cellulose conductive ionic hydrogel for smart wearable devices and thermal actuators. *ACS Appl. Mater. Interfaces.* **2021**, *13* (1), 1353−1366.
(27) Cao, Y.; Morrissey, T. G.; Acome, E.; Allec, S. I.; Wong, B. M.; Keplinger, C.; Wang, C. A transparent, self-healing, highly stretchable ionic conductor. *Adv. Mater.* **2017**, *29* (10), No. 1605099.
(28) Wu, Z.; Yang, X.; Wu, J. Conductive hydrogel-and organo-hydrogel-based stretchable sensors. *ACS Appl. Mater. Interfaces.* **2021**, *13* (2), 2128−2144.
(29) Hu, N.; Hong, B.; Yan, X.; Wu, H.; Zhong, Q.; Qi, D.; Wang, W.; Lei, L.; Fan, H.; Müller-Buschbaum, P. Hybrid Hydrogel-Based Skin Health Monitor for Tracing Solar UV Radiation in Aqueous Environments. *ACS Appl. Polym. Mater.* **2023**, *5* (9), 7528−7538.
(30) Lin, L.; Shen, L.; Zhang, J.; Xu, Y.; Fang, Z.; Müller-Buschbaum, P.; Zhong, Q. Ionic Hydrogels Based Wearable Sensors to Monitor the Solar Radiation Dose for Vitamin D Production and Sunburn Prevention. *ACS Appl. Mater. Interfaces.* **2021**, *13* (38), 45995−46002.
(31) Lu, Y.; Yue, Y.; Ding, Q.; Mei, C.; Xu, X.; Jiang, S.; He, S.; Wu, Q.; Han, J. Environment-tolerant ionic hydrogel-elastomer hybrids with robust interfaces, high transparence, and biocompatibility for a mechanical−thermal multimode sensor. *InfoMater.* **2023**, *5* (4), No. e12409.
(32) Laxminarayan, S.; Rakesh, V.; Oyama, T.; Kazman, J. B.; Yanovich, R.; Ketko, I.; Epstein, Y.; Morrison, S.; Reifman, J. Individualized estimation of human core body temperature using noninvasive measurements. *J. Appl. Physiol.* **2018**, *124* (6), 1387−1402.
(33) Wu, J.; Wu, Z.; Wei, Y.; Ding, H.; Huang, W.; Gui, X.; Shi, W.; Shen, Y.; Tao, K.; Xie, X. Ultrasensitive and stretchable temperature sensors based on thermally stable and self-healing organohydrogels. *ACS Appl. Mater. Interfaces* **2020**, *12* (16), 19069−19079.
(34) Lei, Z.; Wu, P. A supramolecular biomimetic skin combining a wide spectrum of mechanical properties and multiple sensory capabilities. *Nat. Commun.* **2018**, *9* (1), 1134.
(35) An, R.; Zhang, X.; Han, L.; Wang, X.; Zhang, Y.; Shi, L.; Ran, R. Healing, flexible, high thermal sensitive dual-network ionic conductive hydrogels for 3D linear temperature sensor. *Mater. Sci. Eng.* **2020**, *107*, No. 110310.
(36) Wu, Z.; Shi, W.; Ding, H.; Zhong, B.; Huang, W.; Zhou, Y.; Gui, X.; Xie, X.; Wu, J. Ultrastable, stretchable, highly conductive and transparent hydrogels enabled by salt-percolation for high-performance temperature and strain sensing. *J. Mater. Chem.* **2021**, *9* (39), 13668−13679.
(37) Wu, Z.; Ding, H.; Tao, K.; Wei, Y.; Gui, X.; Shi, W.; Xie, X.; Wu, J. Ultrasensitive, stretchable, and fast-response temperature sensors based on hydrogel films for wearable applications. *ACS Appl. Mater. Interfaces.* **2021**, *13* (18), 21854−21864.
(38) Tatiana, N. M.; Cornelia, V.; Tatia, R.; Aurica, C. Hybrid collagen/pNIPAAM hydrogel nanocomposites for tissue engineering application. *Colloid Polym. Sci.* **2018**, *296*, 1555−1571.
(39) Li, Y.; Qin, J.; Bao, H.; Han, Y.; Zeng, X.; Zheng, H.; Huang, Y.; Xia, X.; Dong, Z.; Hu, R.; Liu, Y. Controlled tuning of LCST based on poly (N-isopropylacrylamide)/Hydroxypropyl cellulose

temperature-sensitive hydrogel by electron beam pre-radiation method. *J. Polym. Res.* **2018**, *25*, 19.
(40) Ma, Y.; Lu, Y.; Yue, Y.; He, S.; Jiang, S.; Mei, C.; Xu, X.; Wu, Q.; Xiao, H.; Han, J. Nanocellulose-mediated bilayer hydrogel actuators with thermo-responsive, shape memory and self-sensing performances. *Carbohydr. Polym.* **2024**, *335*, No. 122067.
(41) Jiao, Y.; Lu, Y.; Lu, K.; Yue, Y.; Xu, X.; Xiao, H.; Li, J.; Han, J. Highly stretchable and self-healing cellulose nanofiber-mediated conductive hydrogel towards strain sensing application. *J. Colloid Interface Sci.* **2021**, *597*, 171−181.
(42) Jiao, Y.; Lu, K.; Lu, Y.; Yue, Y.; Xu, X.; Li, J.; Han, J. Highly viscoelastic, stretchable, conductive, and self-healing strain sensors based on cellulose nanofiber-reinforced polyacrylic acid hydrogel. *Cellulose.* **2021**, *28*, 4295−4311.
(43) Ma, J.; Zheng, C.; Lu, Y.; Yue, Y.; Yang, W.; Mei, C.; Xu, X.; Xiao, H.; Han, J. Mussel-adhesive chemistry inspired conductive hydrogel with self-adhesion, biocompatibility, self-recovery and fatigue-resistance performances as flexible sensing electronics. *Compos Part A-Appl. S.* **2024**, *185*, No. 108330.
(44) Hu, Z.; Wang, H.; Li, L.; Wang, Q.; Jiang, S.; Chen, M.; Li, X.; Shaotong, J. pH-responsive antibacterial film based polyvinyl alcohol/poly (acrylic acid) incorporated with aminoethyl-phloretin and application to pork preservation. *Food Res. Int.* **2021**, *147*, No. 110532.
(45) Fu, M.; Sun, Z.; Liu, X.; Huang, Z.; Luan, G.; Chen, Y.; Peng, J.; Yue, K. Highly Stretchable, Resilient, Adhesive, and Self-Healing Ionic Hydrogels for Thermoelectric Application. *Adv. Funct. Mater.* **2023**, *33* (43), No. 2306086.
(46) Liu, D.; Zhou, H.; Zhao, Y.; Huyan, C.; Wang, Z.; Torun, H.; Guo, Z.; Dai, S.; Xu, B. B.; Chen, F. A Strand Entangled Supramolecular PANI/PAA Hydrogel Enabled Ultra-Stretchable Strain Sensor. *Small.* **2022**, *18* (47), No. 2203258.
(47) Wang, Y.; Yu, Y.; Zhao, F.; Feng, Y.; Feng, W. Multi-functional and multi-responsive layered double hydroxide-reinforced polyacrylic acid composite hydrogels as ionic skin sensors. *Adv. Compos. Hybrid Mater.* **2023**, *6* (2), 65.
(48) Luo, J.; Song, T.; Han, T.; Qi, H.; Liu, Q.; Rosenau, T. Multifunctional roles of TEMPO-oxidized cellulose nanofibrils on the enhancement of mechanical and conductive properties of acrylic-based hydrogels for temperature response and human motion sensing. *Chem. Eng. J.* **2024**, *493*, No. 152649.
(49) Xu, S.; Wu, S.; Zhu, R.; Qiu, Z.; Yan, Y. Fully Physically Crosslinked PNIPAM Ionogels with High Mechanical Properties and Temperature-Managed Adhesion Achieved by H_2O/Ionic Liquid Binary Solvents. *Adv. Funct. Mater.* **2024**, No. 2405965.
(50) He, X.; Liu, X.; Yang, J.; Du, H.; Chai, N.; Sha, Z.; Geng, M.; Zhou, X.; He, C. Tannic acid-reinforced methacrylated chitosan/methacrylated silk fibroin hydrogels with multifunctionality for accelerating wound healing. *Carbohydr. polym.* **2020**, *247*, No. 116689.
(51) Sang, C.; Wang, S.; Jin, X.; Cheng, X.; Xiao, H.; Yue, Y.; Han, J. Nanocellulose-mediated conductive hydrogels with NIR photo-response and fatigue resistance for multifunctional wearable sensors. *Carbohydr. Polym.* **2024**, *333*, No. 121947.
(52) Yan, Q.; Zhou, M.; Fu, H. Study on mussel-inspired tough TA/PANI@ CNCs nanocomposite hydrogels with superior self-healing and self-adhesive properties for strain sensors. *Compos. B. Eng.* **2020**, *201*, No. 108356.
(53) Zheng, S. Y.; Ding, H.; Qian, J.; Yin, J.; Wu, Z. L.; Song, Y.; Zheng, Q. Metal-coordination complexes mediated physical hydrogels with high toughness, stick-slip tearing behavior, and good processability. *Macromolecules.* **2016**, *49* (24), 9637−9646.
(54) Dang, X.; Fu, Y.; Wang, X. Versatile Biomass-Based Injectable Photothermal Hydrogel for Integrated Regenerative Wound Healing and Skin Bioelectronics. *Adv. Funct. Mater.* **2024**, 2405745.
(55) Gong, X.; Fu, C.; Alam, N.; Ni, Y.; Chen, L.; Huang, L.; Hu, H. Preparation of hemicellulose nanoparticle-containing ionic hydrogels with high strength, self-healing, and UV resistance and their applications as strain sensors and asymmetric pressure sensors. *Biomacromolecules.* **2022**, *23* (6), 2272.
(56) Peng, J.; Cao, D.; He, Z.; Guo, J.; Hapala, P.; Ma, R.; Cheng, B.; Chen, J.; Xie, W. J.; Li, X. Z.; Jelínek, P.; Xu, L. M.; Gao, Y. Q.; Wang, E. G.; Jiang, Y. The effect of hydration number on the interfacial transport of sodium ions. *Nature.* **2018**, *557* (7707), 701−705.
(57) Wang, J.; Chen, Z.; Li, X.; Liu, M.; Zhu, Y.; Jiang, L. Plastic-like hydrogels with reversible conversion of elasticity and plasticity and tunable mechanical properties. *ACS Appl. Mater. Interfaces.* **2019**, *11* (44), 41659−41667.
(58) Zheng, C.; Lu, K.; Lu, Y.; Zhu, S.; Yue, Y.; Xu, X.; Mei, C.; Xiao, H.; Wu, Q.; Han, J. A stretchable, self-healing conductive hydrogels based on nanocellulose supported graphene towards wearable monitoring of human motion. *Carbohydr. Polym.* **2020**, *250*, No. 116905.
(59) Zhu, C. N.; Li, C. Y.; Wang, H.; Hong, W.; Huang, F.; Zheng, Q.; Wu, Z. L. Reconstructable gradient structures and reprogrammable 3D deformations of hydrogels with coumarin units as the photolabile crosslinks. *Adv. Mater.* **2021**, *33* (18), 2008057.
(60) Hoshino, K. I.; Nakajima, T.; Matsuda, T.; Sakai, T.; Gong, J. P. Network elasticity of a model hydrogel as a function of swelling ratio: from shrinking to extreme swelling states. *Soft matter.* **2018**, *14* (47), 9693−9701.
(61) Park, J.; Kim, T. Y.; Kim, Y.; An, S.; Kim, K. S.; Kang, M.; Kim, S. A.; Kim, J.; Lee, J.; Cho, S.; Seo, J. A mechanically resilient and tissue-conformable hydrogel with hemostatic and antibacterial capabilities for wound Care. *Adv. Sci.* **2023**, *10* (30), No. 2303651.
(62) Zhang, X.; Chen, L.; Zhang, C.; Liao, L. Robust near-infrared-responsive composite hydrogel actuator using Fe^{3+}/tannic acid as the photothermal transducer. *ACS Appl. Mater. Interfaces.* **2021**, *13* (15), 18175−18183.
(63) Shi, J.; Hao, X.; Yang, H.; He, Z.; Lu, J.; Li, Y.; Luan, L.; Zhang, Q. A biguanide chitosan-based hydrogel adhesive accelerates the healing of bacterial-infected wounds. *Carbohydr. Polym.* **2024**, *342*, No. 122397.
(64) Wang, Y.; Liu, Y.; Yang, H.; Fu, Y.; Huan, L.; Zhu, F.; Wang, D.; Liu, C.; Han, D. Thermal responsive sodium alginate/polyacrylamide/poly (N-isopropylacrylamide) ionic hydrogel composite via seeding calcium carbonate microparticles for the engineering of ultrasensitive wearable sensors. *Int. J. Biol. Macromol.* **2024**, *280*, No. 135909.
(65) Yamawaki, Y.; Shirawachi, S.; Mizokami, A.; Nozaki, K.; Ito, H.; Asano, S.; Kanematsu, T. Phospholipase C-related catalytically inactive protein regulates lipopolysaccharide-induced hypothalamic inflammation-mediated anorexia in mice. *Neurochem. Int.* **2019**, *131*, No. 104563.
(66) Wan, J. J.; Qin, Z.; Wang, P. Y.; Sun, Y.; Liu, X. Muscle fatigue: general understanding and treatment. *Exp. Mol. Med.* **2017**, *49* (10), No. e384.
(67) Li, H.; Chng, C. B.; Zheng, H.; Wu, M. S.; Bartolo, P. J. D. S.; Qi, H. J.; Tan, Y. J.; Zhou, K. Self-Healable and 4D Printable Hydrogel for Stretchable Electronics. *Adv. Sci.* **2024**, *11* (13), No. 2305702.
(68) Yamada, T.; Hayamizu, Y.; Yamamoto, Y.; Yomogida, Y.; Izadi-Najafabadi, A.; Futaba, D. N.; Hata, K. A stretchable carbon nanotube strain sensor for human-motion detection. *Nat. Nanotechnol.* **2011**, *6* (5), 296−301.

https://doi.org/10.1021/acsapm.4c03794
ACS Appl. Polym. Mater. 2025, 7, 2529−2540